2nd International Conference on the Material Point Method for Modelling Soil-Water-Structure Interaction

Anura3D
MPM Research Community

Paper number: mpm2019.10
www.anura3d.com
www.mpm2019.eu

Implementation of non-trivial boundary conditions in MPM for geotechnical applications

G.Remmerswaal[1,*], M.Bolognin[1], P.J. Vardon[1], M.A. Hicks[1], A. Rohe[2]
[1]Faculty of Civil Engineering and Geosciences, Delft University of Technology, Delft, The Netherlands
[2]Deltares, Delft, The Netherlands

[*] E-mail: g.remmerswaal@tudelft.nl

ABSTRACT

This paper describes current work on the implementation of non-trivial boundary conditions(BCs) for improvingthe general applicability of the Material Point Method (MPM) to geotechnical boundary values problems. It summarises novel boundary treatments (non-trivial BCs) in MPM for (i) flow conditions, as well as (ii) the application of a surface traction on a moving boundary for solid materials. Both treatments are required, for example, to estimate the consequence of slope failure in geotechnical engineering. The flow condition BCs have been used to simulate a subcritical flow and the surface traction BC has been applied on top of aslope leading to failure. Both examples show that these new treatments are useful in solving practical problems.

KEY WORDS: Boundary conditions; Geotechnical engineering practice; Material Point Method; Slope stability.

INTRODUCTION

In continuum mechanics, boundary value problems usually involve differential equations (e.g. mass and momentum conservation) with a set of additional constraints, namely boundary conditions (BCs). The Material Point Method (MPM), which decouples mass from the background grid, has proven to be useful in many geotechnical large deformation problems(Sulsky et al., 1994).

Despite the abundance of small deformation models, both analytical as well as numerical, geotechnical design is often limited to a strength analysis. Especially in slope stability theory, current practice is limited to the computation of factors of safety. Applying MPM to slope stability theory enables a quantitative and qualitative estimation of the consequence of failure, which, for example, is required for risk assessment, vulnerability analyses and displacement design criteria.

Even though MPM has been already applied to many slope stability problems(Andersen et al.,2010;Soga et al.,2016; Wang et al., 2016; Coelho et al.,2018), these analyses often directly applied the BCs from the Finite Element Method (FEM) on an edge of the background grid. Nowadays, MPM applications are often limited by (usuallyfixed) BCs located at the grid edges. However, BCs are more commonly associated with the mass in solid mechanicsor often flux-based in fluids, i.e. they are decoupled from the grid in MPM. Therefore, for a general application of MPM to slope stability problems, non-trivial BCs are required as well (Cortis et al.,2018).

This paper summarises novelboundary treatments in MPM for flow conditions (Zhao et al.,2018) and a novel method for the application of a surface traction on a moving boundary (Remmerswaal,2017). Flow boundary conditions maybe used to simulate, for example, flow within a slope or erosional and depositional processes (Shields, 1936; Einstein, 1950;etc.). A surface traction can be used to apply a load, for example on top of a slope, which remains present during failure. This traction could, for example, represent a building founded on top of an embankment.

IN/OUTFLOW BCS FOR UNIFORM AND NON-UNIFORM FLOWS

Recent advances in MPM theory have made this method a robust unified framework with efficient and versatile coupling techniques for solid-fluid-structure-gas interaction and large deformations, especially when compared to more established civil engineering methods such as Smoothed Particle Hydrodynamics (SPH) (Yan et al., 2018). To reduce the computational cost of MPM, large domains are often truncated and confined between artificial boundaries (ABCs)(Zhao & Liang, 2016; Bolognin et al., 2017; Martinelli et al., 2017). The locationof the required ABCs can be fabricated by intuition, experience, asymptotic behaviour and numerical experimentation (Papanastasiou et al., 1992). For truncation of the domain in fluid flows, ABCs are required which allow the fluid to flow in and out of the area of interest. This paper describes the implementation of an MPM BC, which improves the conditions under which material points are introduced or removed at the boundaries. The novel BC treatment thereby allows the description of well-posedproblems that are able to simulate truncated fluid flow mechanics.

To simulate a segment of a flow, the boundary must allow mass to enter andleave the domain ata predefined flow rate, and (simultaneously) control the pressure imposed from the water outside the boundary. For a solvable governing equation, all boundariesare required to only have one BC imposed. Moreover, as mass is entering and leaving the domain (in MPM), material points(MPs) must be introduced or removed (to ensure mass continuity). In flow conditions at least one BC should control the kinematics, i.e. fix the acceleration or velocity, otherwise the problem is not well-posed. However, the inflow and outflow conditions cannot simultaneously control kinematics, as physically impossible situations may then arise (e.g.not enough mass in the domain to satisfy the BCs).Many flow segments finishin either subcritical hydraulic conditions or zero pressure conditions, so a pressure boundary is more appropriate for the outflow boundary. Consequently, the inflow boundary has been selected to control the kinematics.

The novel in/outflow BCs are respectively very similar to the classic flux (velocity) and traction controlled (pressure) BCs of FEM. The difference is that due to the material discretisation into MPs, the MPs move in and out of the domain. This means specific methods for the Eularian component must be developed.

In order to impose a velocity and fixed (zero) acceleration, a zero acceleration is applied on the nodes of the boundary condition, see Figure 1a. In addition, additional material points must be added. To facilitate this an additional row of ghost elements (inflow elements) are added immediately next to the domain. Material points are added in these elements such that the water density is maintained. These points are given an initial velocity of the required flux and a fixed acceleration. Neither the velocity nor the acceleration are changed until the points enter the domain. Details of the implementation can be found in (Zhao et al., 2018).

Conversely, an outflow BC needs to impose a prescribed force (Neumann BCs), representing, for example, hydrostatic pressure (Figure 1b), in the same manner as FEM. Also in this case an additional set of elements was used in order to remove the points that leave the computational domain. As soon as material points enter these elements they are removed from the calculation.

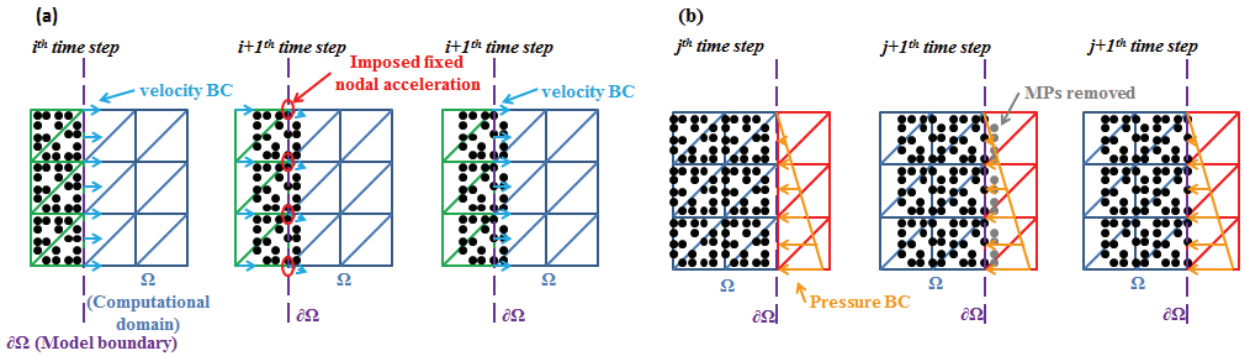

Figure 1 Illustration of the (a) inflow BC with inflow elements (green), and (b) outflow BC with outflow elements (red) (Zhao et al., 2018).

In this paper a steady uniform inflow is considered for the inflow boundaries and a fixed pressure is consideredfor the outflow boundaries. However, it would be straightforward to update the procedure for a temporally varying inflow.

In order to validate the theoretical formulation and numerical implementation of in/out flow BCs, a subcriticalrectangular open channel flow problem has been simulated. An initiallyempty domain is considered of 0:15 x 0:15 x 0:01 m, in the *x*-, *y*-, *z*-directions, with frictionlesswalls, a prescribed horizontal inflow velocity of 1.0 m/s and a zero acceleration along the inflowboundary as indicated in Fig. 2a. The domain is discretised by line artetrahedral elements and it is modelled with only one element in the*z*-direction since it is an axisymmetric problem with only the *x*- and *y*-directions shown in Fig.2. A band of outflow elements is attached on the right side of the computational mesh with aprescribed hydrostatic pressure on its nodes. Outflow elements and their BCs are only activated when MPsenter the adjacent elements. The water is modelled by a simple Newtonian compressible constitutivemodel. It has an initial density $\rho_0 = 1$ Mg/m^3, dynamic viscosity $\mu = 1$ GPa·s and bulkmodulus $K = 20$ MPa. The water bulk modulus was reduced by a factor of 100 from reality inorder to increase the time step size, as an explicit time integration scheme has been adopted.

Fig. 2 shows the simulation results in terms of (b) pressure and (c) velocity at different time steps. During the initial time interval of about 0.8s atransient flow is observed. The water front resembles a dam break simulation with constant water level during this period, until it reaches the wall, where in this case the material points are removed. After the initial interval, a steady uniform flow is achieved and maintained until the simulation time is complete. Note that the prescribed traction BC at the outflow boundary nodes causes unreasonably high pressures near the bottom when the flow is not yet fully developed, which is especially evident at 0.15 s and 0.20 s. This is caused by the prescribed hydrostaticpressure which is currently initiated based on the final water depth. As the calculation continues, and the outlet water level keeps rising, this inconsistency vanishes. This phenomenon can be avoided if the hydrostatic pressure at the outflow elements would be updated during the calculation based on the water depth. However, the purpose of the present simulation is to indicate the capabilities of the proposed in/outflow BCs by developing and maintaining a steady uniform flow. The BCs are capable of fulfilling this purpose as, after 0.8 s, a constant velocity, a hydrostatic pressure and a horizontal free surface are achieved.

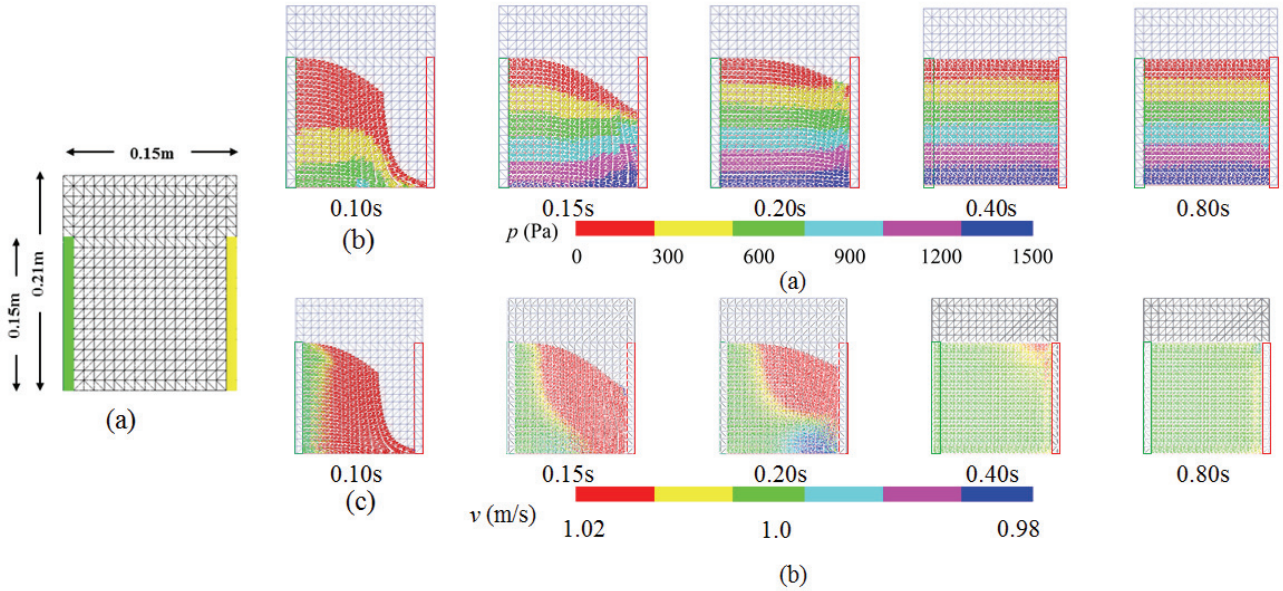

Figure 2 (a) Computational mesh of a rectangular channel and application of in/outflow BCs for the simulation of a subcritical flow. Representation of the fluid flow converging to a steady solution enforced by the downstream BC; (b) pressure field; (c) velocity field at different time steps (Zhao et al., 2018).

TRACTION BOUNDARY CONDITION FOR MOVING BOUNDARIES

In FEM, the nodes of the mesh coincide with the boundary, and the location of the edge of a continuum body is always known(Cortis et al.,2018). Therefore, application of most BCs to the boundaries of a continuum body in FEM is trivial. However, application of BCs to moving boundaries in MPM is a challenge, as the location of a body boundary is generally unknown a priori in MPM. Indeed, in MPM the MPs are by definition not located at the body boundaries as they represent centres of mass. Moreover, due to the fact that the MPs flow through the background grid, free boundaries are not guaranteed to coincide with the background grid nodes. So, it is not trivial to use the MPs or the background grid nodes for the application of BCs. Certain BCs, for example completely fixed BCs at the edge of a structure, can be easy to align along a background grid edge. The application of BCs at these location is generally similar to FEM. Therefore, the focus in this section is on boundary conditions which are not aligned with the background grid edges. Indeed, moving boundaries by their nature are unaligned boundaries (at least during many steps of a simulation). Fixed displacement(unaligned) boundaries have been addressed by Cortis et al. (2018); here traction boundaries are addressed.

Even though the MPs are not located at the boundary, BCs have generally been applied to material points located close to the boundary in the initial condition (e.g. Wang et al., 2018). For simplicity, the BCs are applied at these MPs during the entire deformation process, regardless of the distance to the body boundary. In contrast, the approach taken in this paper is to apply the BC exactly at the boundary, by distributing it to the background grid nodes. This removes unnecessary inaccuracies and means that models will not have to be unnecessarily refined.

To apply the traction condition at the nodes, FEM shape functions are used to map the condition from the body boundary onto the nodes. This mapping is the same integration along the boundary of the continuum body which is used in FEM (and for aligned BCs in MPM). However, for aligned BCs this integration involves only the nodes at the boundary, whereas for unaligned BCs all the nodes surrounding the boundary are required. For moving boundaries the location of the boundary must be known in order to apply the BC. An edge detection method is therefore used to locate the boundary based on the information stored at the MPs(Remmerswaal, 2017).

The edge detection method, called the Proximity Field Method (PFM), is an implementation of the Level Set Method(Sethian, 1996). In PFM a proximity field is created by a summation of kernel functions around all MPs. These kernel functions can deform according to the deformations computed at the MPs, which allows for an accurate representation of the material domain. The edge of the domain is found by comparing the field with a threshold. This threshold is defined in the initial condition to achieve a good fit between the material boundary and the edge detected by PFM, as shown in Figure 3a. Using this threshold the points at which the material boundary crosses an edge of the background grid are found. Finally, the edge is constructed by connecting these points on the background grid with composite Bézier curves (Figure 3b). The edge can thereby be constructed from polynomial sections of each order.

Once the location of the edge has been found, FEM shape functions are used to integrate the surface traction from the boundary to the nodes surrounding the edge (Figure 3c). Gaussian integration along the edge can be used to compute the nodal forces, which are directly applied in the MPM governing equations. The traction can be defined normal to the surface, tangential to the surface or along a predefined direction independent from the angle of the surface. The traction in Figures3b and 3c has been defined to be in the vertical direction.

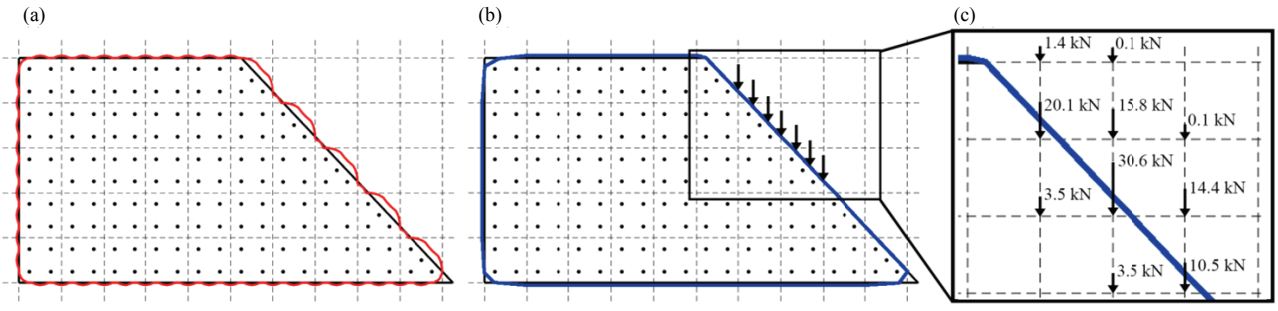

Figure 3Illustration of a surface traction BC on a free boundary: (a) contour of proximity field, (b) detected edge after segmentation of the contour with the background grid, and (c) external loads applied to the nodes due to a vertical traction of 50 kPa alonga part of the free boundary.

In order to demonstrate the capabilities of PFM, the effect of a surface traction on top of a soil slope has been simulated. A 10 m high, 45° clay slope, founded on a 3 m thick clay layer, is loaded under gravity. The slope and foundation layer are placed on top of a fixed boundary representing a stiff stratum. After the initial stresses have been generated an additional surface traction$q$ is applied over a length of 5 m. This traction can represent, for example, a small building founded on top of the slope. Two cases have been studied, in which q is applied between 5-10 m (called case 1) and 10-15 m (called case 2) from the crest. During deformation the horizontal location of q remains fixed, i.e. it is always applied between either 5-10 m or 10-15 m from the crest. However, q follows the vertical deformation of the slopeas it is applied on top of the edge computed with PFM. The traction has been fixed to be in the vertical direction. Furthermore, to investigate if PFM correctly computes the effect of different surface tractions, multiple simulations have been performed in which q has been varied, i.e.q = 0, 20, 30, 50 or 100 kPa. The soil has a Young's modulus of 1000 kPa and a Poisson's ratio of 0.45.An undrained cohesion (c_u) softening Von Mises constitutive model has been used. The strength of the soil has been varied, with an initial cohesion ofc_u^i = 35, 40, 45 or 50 kPa, to study the effect of a surface traction on slopes which are either stable or unstable under their own weight. The residual cohesion is fixed to $c_u^r = 0.5c_u^i$.

All models were setup to run a simulation of 60 s. However, in some analyses of case 1, a single material point detached from the continuum body and the simulation ended prematurely. This was due to the geometry and application of the surface traction, where a large stress concentration occurs due to the load being applied at the location where the gravitational slip surface cuts through the top of the slope. This occurred in four simulations (c_u^i= 40 or 45 kPa and q = 50 or 100 kPa). However, most of the deformation occurred before the premature end in all these simulations and the effect on the results shown in this paper is therefore small.

Figure 4 shows the MPs at the end of a simulation of case 1,with an initial cohesion $c_u^i$of 50 kPa and an applied traction q = 100 kPa. Furthermore, the edge detected with PFM for this simulation is given in red. In general, the detected edge well representsthe boundary of the domain. However, sharp corners are rounded and small gaps can occur within the material. Smoothing techniques, such as Gaussian smoothing, can be used to reduce the occurrence of these gaps. Unfortunately, sharp corners are rounded further by Gaussian smoothing.The blacklineshows the edge detected for the same slope loaded only by gravity, i.e. q = 0 kPa, which remains stable. Finally, the green line represents the same slope loaded by the same load (q = 100 kPa), but atthe location of case 2.A slope failure is still observed for case 2, but the deformation is much smaller when compared to case 1.

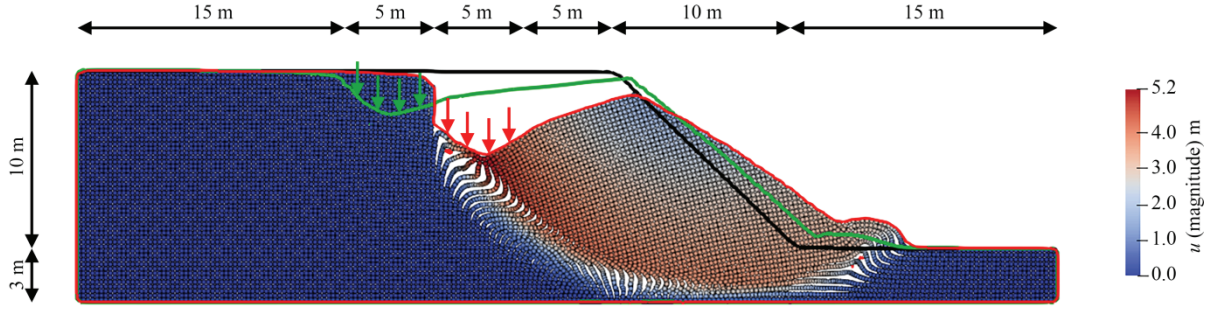

Figure 4End of a simulation with c_u^i= 50 kPa;MPs and their colour represent the displacement for q = 100 kPa (case 1); PFM edge for q = 100 kPa (case 1) coloured in red;PFM edge for q = 100 kPa (case 2) coloured in green;PFM edge for$q$ = 0 kPa coloured in black.

The maximum vertical displacement $u_y$is presented in Figure 5. For q = 0 kPa, large deformations, i.e. slope failures, are observed for the two weakest materials. For increasing q the maximum deformation tends to increase as shown in Figure 5. Figure 5a show that for case 1, the maximum displacements increase with an increase of$q$, because the surface traction is applied on top of the gravitational slip surface. However, for case 2 the maximum displacement for q = 20 kPaslightly decreases compared to a slope without a surface traction (see Figure 5b). The surface traction causes heaving of the soil on either side of the traction. Due to the fact that q is applied to the side of the location of the gravitational slip surface, the maximum deformation is reduced by the heaving caused by the surface traction.An increase of q above 30 kPa causes deformations beneath the tractionwhich exceed the maximum deformation caused by the gravitational failure for q = 0 kPa. Therefore, for q larger than 30 kPathe maximum deformation once again increases compared to q = 0 kPa as shown in Figure 5b.

For the stronger soils (c_u^i= 45 or 50 kPa) limited deformations are observed for low values of q. After $q$has reach a certain value, depending on the strength of the soil, a sharp increase in the deformation is observed, i.e. a slope failure occurred. PFM can therefore be used to compute a safety limit for q,while also providing the behaviour when this limit has been reached. Decreasing the step size in$q$ will improve the accuracy of the limit load. Finally, as expected the maximum deformations in case 1 are larger than in case 2, because the load is applied on top of the gravitational slip surface in the former case whereas it is to the side of the slip surface in the latter. Due to the adopted step size in$q$a difference in the safety limit cannot clearly be observed.

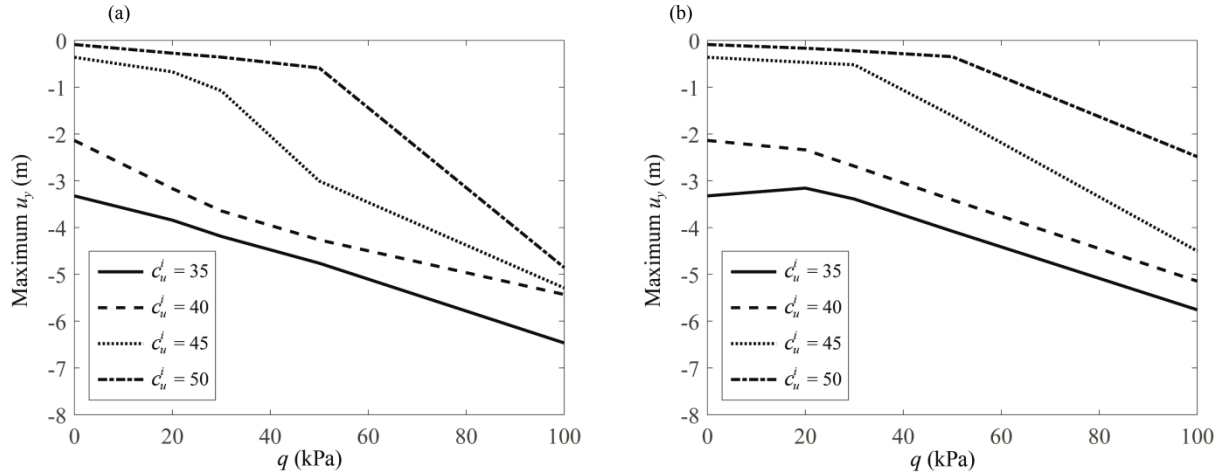

Figure 5Maximum vertical deformation for a slope loaded by a vertical surface traction for various c_u^i(kPa) and q, (a) case 1, (b) case 2.

CONCLUSIONS

Novel BCs have been outlined, which allow MPM to be more generally applied in hydro-geotechnical applications. Two numerical applications have been presented, in which these BCs are shown to give reasonable results. However, further evaluation is required to determine the accuracy of the BCs. Being able to prescribe in/outflow BCs (i) allows true steady-state conditions,(ii) reduces computational cost, (iii) simplifies the geometry, and (iv) improves the general applicability of the method.PFM has been shown to be capable of computing a limit load in MPM, while also providing the behaviour of the structure once this limit load has been reached. Both the in/outflow BCs and PFM can be further developed to increase the general applicability of MPM.

ACKNOWLEDGEMENTS

The Authors are thankful for the technical support from the MPM research group at Deltares, The Netherlands. The Anura3D software is made available by the Anura3D MPM Research Community. Marco Bolognin is grateful for the financial support by the NWO Project “MPM-FLOW: Understanding flow slides in flood defences” (Grant No. 13889). Guido Remmerswaal is part of the “Perspectief research programme All-Risk” with project number P15-21 4, which is (partly) financed by NWO Domain Applied and Engineering Sciences.

REFERENCES

Andersen S & Andersen L. (2010). Modelling of landslides with the material-point method.*Computational Geosciences,* 14(1), 137–147.

Bolognin M, Martinelli M, Bakker KJ & Jonkman SN.(2017). Validation of material point method for soil fluidisation analysis. *Journal of Hydrodynamics, Ser. B*, 29(3), 431–437.

Coelho BZ, Bolognin M, Nuttall JD, Rohe A &Aboufirass A. (2018). Assessment of dike safety within the framework of large deformation analysis with the material point method. *Proceedings of Numerical Methods in Geotechnical Engineering IX*, Porto, Portugal, 657–665.

Cortis M, Coombs WM, Augarde CE, Brown MJZ, Brennan A & Robinson S. (2018). Imposition of essential boundary conditions in the material point method. *International Journal for Numerical Methods in Engineering*, 113, 130–152.

Einstein HA. (1950). *The bed-load function for sediment transportation in open channel flows*. Report No. 1026, United

States Department of Agriculture Soil Conservation Service, Washington, D.C., USA.
Martinelli M, Rohe A & Soga K. (2017).Modelingdike failure using the material point method. *Procedia Engineering*, 175,341–348.
Papanastasiou TC, Malamataris N&Ellwood K. (1992). A new outflow boundary condition. *International Journal for Numerical Methods in Fluids*, 14(5), 587–608.
Remmerswaal G.(2017). *Development and implementation of moving boundary conditions in the material point method.* MSc Thesis, Faculty of Civil Engineering and Geosciences, Delft University of Technology, Delft, The Netherlands.
Sethian JA. (1996). Theory, algorithms, and applications of level set methods for propagating interfaces. *ActaNumerica*, 5, 309–395.
Shields A. (1936). *Application of similarity principles and turbulence research to bed-load movement*. Translation of the Ph.D. Thesis of A. Shields, Publication No. 167 Hydrodynamics Laboratory, CalTech Library, Pasadena, USA.
Soga K, Alonso E, Yerro A, Kumar K&Bandara S. (2016). Trends in large-deformation analysis of landslide mass movements with particular emphasis on the material point method. *Geotechnique*, 66(3), 248–273.
Sulsky D, Chen Z & Schreyer HL.(1994). A particle method for history-dependent materials.*Computer Methods in Applied Mechanics and Engineering*, 118(1–2),179–196.
Wang B, Vardon PJ & Hicks MA. (2016). Investigation of retrogressive and progressive slope failure mechanisms using the material point method.*Computers and Geotechnics*, 78, 88–98.
Wang B, Vardon PJ & Hicks MA. (2018). Rainfall-induced slope collapse with coupled material point method. *Engineering Geology*, 239,1–12.
Yan X, Li C, Chen X & Hu S. (2018). MPM simulation of interacting fluids and solids. *Computer Graphics Forum*, 37(8), 183–193.
Zhao X, Bolognin M, Liang D, Rohe A, & Vardon PJ (2018). Development of in/outflow boundary conditions for MPM simulation of uniform and non-uniform open channel flows. *Computers & Fluids*, 179, 27–33.
Zhao X & Liang D. (2016). MPM Modelling of seepage flow through embankments. *In International Ocean and Polar Engineering Conference,*Rodos, Greece, 1161–1165.